ELECTROMAGNETIC COMMUNICATION LABORATORY
TECHNICAL REPORT NO. 85-6

CHARACTERIZATION OF MICROSTRIP DISCONTINUITIES IN THE TIME AND FREQUENCY DOMAINS

U. Feldman
R. Mittra

Supported by

NASA Lewis Research Center
Contract No. NCC-3-38

ELECTROMAGNETIC COMMUNICATION LABORATORY
DEPARTMENT OF ELECTRICAL AND COMPUTER ENGINEERING
UNIVERSITY OF ILLINOIS AT URBANA-CHAMPAIGN
URBANA, ILLINOIS 61801

UILU-ENG-85-2565

Electromagnetic Communication Laboratory Report No. 85-6

CHARACTERIZATION OF MICROSTRIP DISCONTINUITIES IN THE TIME AND FREQUENCY DOMAINS

by

U. Feldman and R. Mittra

Technical Report

September 1985

Electromagnetic Communication Laboratory
Department of Electrical and Computer Engineering
University of Illinois at Urbana-Champaign
Urbana, Illinois 61801

This report was supported by NASA Lewis Research Center under contract NCC-3-38.

ABSTRACT

In this experimental study, a number of impedance transitions and interconnections to a microstrip were designed and investigated. The double-step discontinuity on a microstrip was studied in detail, and a procedure was developed to design these structures. Their response was determined by making measurements in both the frequency and time domains in a consistent and repeatable manner. The time-domain presentation of the data was the most useful feature of the measuring system. All undesirable signal components were filtered out through the use of gating functions. In this study, theoretically computed results were verified experimentally.

TABLE OF CONTENTS

1. INTRODUCTION

The operation of communication systems at microwave frequencies has created the need for adequate waveguiding circuitry. Hence, the shielded microstrip line is often used to transfer microwave signals between components and other waveguiding structures. Microwave circuits are often placed within a closed cavity or inside a waveguide; Figure 1 shows a shielded microstrip cross-section. This configuration offers certain advantages: reduced size, weight, and cost combined with improved electrical performance, manufacturing uniformity and reliability [1]. Analysis of the discontinuities encountered when using planar guides is quite difficult, because there are no closed-form solutions for the fields which can exist in these structures. Thus, the purpose of this project is to characterize several stepwise discontinuities in the width of microstrip lines from an experimental point of view.

In particular, the double-sided step was chosen for this study for its simplicity to construct and for ease of measurement. Such discontinuities are readily encountered in filters, impedance transformers, and interfaces with active devices.

Primary considerations have been the consistency and repeatability of the experiments. The linear dimensions of the test fixture are within a tolerance of 0.002". The best materials and components available were used in order to satisfy specific

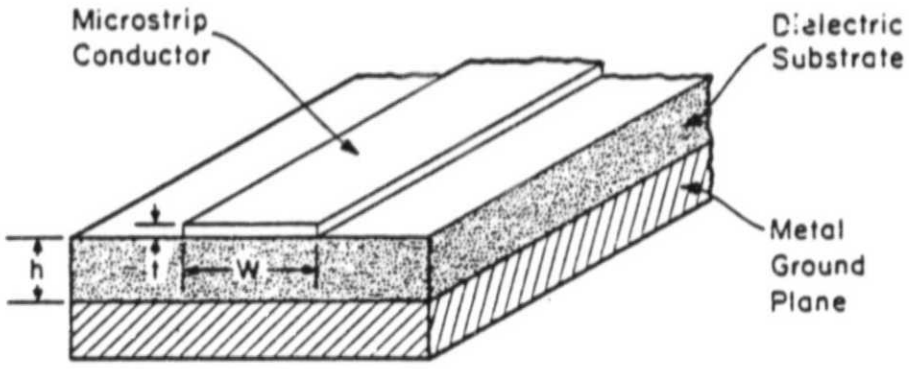

Figure 1. Microstrip cross-section.

electrical and mechanical requirements, namely, low loss, uniformity, and ease of fabrication. From the measured data of a carefully constructed line, it is possible to determine the capacitance at the discontinuity. The optimum parameters determined by this procedure could then be used to maximize the effects of the step discontinuity over the frequency range, from 45 MHz up to 18 GHz.

The test setup utilized throughout this project included sophisticated computer-controlled instrumentation. Preliminary designs and evaluation of performance tests were made on an HP8408 Automated Network Analizer (ANA) system. During the final stage of the program, more accurate measurements were made on an HP8510 ANA system. These systems provided reliable operation up to 18 GHz. One of the most significant aspects of this experimental program has been the study of the microstrip discontinuities in the time domain. From the reflection data obtained, the corresponding time-domain responses could be interpreted using conventional time domain reflectometer techniques.

The repeatability of the experiments was fundamental for the success of the study. For this reason, extreme care was taken in conceiving the design, assembly and measurement procedures.

2. PRELIMINARY CONSIDERATIONS

There are some fundamental problems associated with microstrips which have to be addressed before any designs are completed. These effects, which generally increase in severity as the operating frequency is raised [2], include dielectric and conductor losses, dispersion, and non-TEM mode propagation.

2.1 Dispersion

The analysis presented in this report has been based on a quasi-TEM mode of propagation. This is a valid quasi-static approximation of a dynamic structure at frequencies where the guide dimensions are small relative to the guide wavelength. However, at frequencies where the dimensions of the structure are comparable to the guide wavelength, the effective dielectric constant and characteristic impedance of a microstrip begin to decrease with frequency, thus, making the microstrip dispersive. This dispersive characteristic is due to propagation of non-TEM modes [3].

The propagation velocity and characteristic impedance for the 50 Ω microstrip line designed, as described in Chapter 3, were calculated by Farr using a spectral Galerkin technique [4]. From the values given in Table 1, it can be inferred that within the operating range, up to 12 GHz, the fluctuations in propagation velocity and characteristic impedance were well under 5%. For this reason, for frequencies under 12 GHz, the microstrip lines used throughout the experiment can be considered to be non-dispersive.

Table 1

Propagation characteristics for 50 Ω microstrip

f (GHz)	β (rad/m)	V_p (10^8m/sec)
8	229.9	2.19
10	288.4	2.18
12	336.1	2.24
15	436.1	2.16

2.2 Frequency of operation

The range of frequency over which measurements were taken was determined by two factors. The upper limit was set by the effects of the losses and by the increasingly dominant effect of non-TEM mode propagation. Moreover, the equipment provided reliable operation up to 18 GHz. Hence, it was decided to operate below 12 GHz since single-mode propagation was possible. For frequencies under 12 GHz, losses remained at 0.05 dB per centimeter, only the dominant TEM mode propagated, and the parts could be machined to the specified tolerance. Even though it was decided to operate up to 12 GHz, the measurements were extended up to 18 GHz to evaluate the effects of the non-TEM modes.

In the design of the experimental setup, the effects of the discontinuities had to be maximized relative to the other existing anomalies, such as connectors and adapters. For practical purposes, the connectors and adapters are not ideal and will cause perturbations in the fields, though these effects can be minimized or isolated by techniques that are explained in Chapter 4.

2.3 Non-TEM mode of propagation

In most microstrip applications, only the dominant quasi-TEM mode of operation is desirable; for this reason, guide dimensions have to be maintained well under the guide wavelength. The maximum frequency of operation in a microstrip line is limited by the excitation of propagating non-TEM waves in the form of surface waves and transverse resonances within the guide; in this case, the guide dimensions become comparable to the guide wavelength. This effect becomes predominant, for a fixed characteristic impedance, when either the substrate thickness or dielectric constant is increased [5]. For the configuration under study, the cutoff frequencies for non-TEM modes were computed by Farr using a spectral Galerkin technique [6]. Within the usable operating bandwidth up to 12 GHz, no higher-order modes will propagate. At frequencies above 12 GHz, non-TEM modes start to propagate. The effects of these modes are currently being evaluated.

2.4 Losses

Two major dissipative effects occur in microstrip guides, namely, conductor loss and substrate or dielectric loss. As shown by Pucel [7], conductor loss may be approximated by

For $1/2\pi < W/h \leq 2$,

$$\alpha_c = \frac{8.68\ R_s}{2\pi\ Z_o\ h} \cdot P \cdot Q \quad dB/km \qquad (1)$$

For $W/h \geq 2$,

$$\alpha_c = \frac{8.68\ R_s}{Z_o\ h} \cdot Q \cdot \left[\frac{W_e}{h} + \frac{2}{\pi} \cdot \ln\left\{2\pi e \cdot \left(\frac{W_e}{2h} + 0.94\right)\right\}\right]^{-2} \cdot$$

$$\cdot\left[\frac{W_e}{h} + \frac{W_e/\pi h}{0.94 + W_e/2h}\right] \quad dB/cm \qquad (2)$$

where

$$P = 1 - \left(\frac{W_e}{4h}\right)^2$$

$$Q = 1 + \frac{h}{W_e} + \frac{h}{\pi W_e} \cdot \left(\ln\frac{2h}{t} - \frac{t}{h}\right)$$

$$\frac{W_e}{h} = \frac{W}{h} + \frac{t}{\pi h} \cdot \left(1 + \ln\frac{2h}{t}\right)$$

$$\epsilon_{eff} = \frac{\epsilon_r + 1}{2} + \frac{\epsilon_r - 1}{2} \cdot (1 + 12 \cdot h/W)^{-1/2} \qquad (3)$$

Referring back to Figure 1, W/h is the line width to substrate ratio, W_e is the effective width, t is the strip thickness and R_s is the surface resistance of copper. From these expressions it can be seen that, for a fixed characteristic impedance, conductor loss decreases inversely with substrate thickness, and increases with the square root of the frequency. This is to be expected, due to the skin effect.

For a 50 Ω line, the conductor loss at 12 GHz was calculated to be 0.0145 dB/cm.

The dielectric loss for a material can be calculated using the expression derived by Welch and Pratt [8]:

$$\alpha_D = 27.3 \cdot \frac{\epsilon_R}{\sqrt{\epsilon_{eff}}} \cdot \frac{\epsilon_{eff}-1}{\epsilon_R-1} \cdot \frac{\tan\delta}{C} \cdot f \quad dB/cm \qquad (4)$$

where C is the free-space wave propagation velocity and $\tan\delta$ is the loss tangent for the material. It can be seen from this expression that dielectric loss is directly proportional to the relative dielectric constant. For a constant characteristic impedance line, an increase in ϵ_R results in stronger fields, which, in turn, produces increased ohmic loss.

For the 50 Ω line, dielectric loss at 12 GHz, computed using equation (4), was 0.0118 dB/cm.

Considering conductor and dielectric losses alone, the overall losses total less than 0.03 dB/cm of attenuation at 12 GHz. This is a small number relative to the absolute magnitude of the parameters being measured, i.e., 10 dB and higher and, thus, can be neglected for frequencies below 12 GHz.

The choice of an adequate substrate material required an evaluation of the losses. For a fixed characteristic impedance and fixed thickness, a high relative dielectric constant results in a narrow-line width and a short guide wavelength, with inherently high loss. On the other hand, a low dielectric constant results in a wide line and a long guide wavelength, with significantly lower dielectric loss. Conductor loss remains constant.

Another parameter having a significant effect on the loss is the thickness of the substrate. In a microstrip, the field distribution is confined to the dielectric substrate; the thinner the substrate, the more dense and strong the field lines become, and the higher the losses. For a fixed ϵ_r, a thin board results in a highly lossy, narrow line, whereas a thicker board results in a low loss, but wide line.

With all these considerations in mind, 1/2 ounce, copper clad, RT/Duroid 5880 was selected as a substrate material. The low ϵ_r of 2.2 and thicknes of 0.031" represented a good compromise between loss and size. Some added advantages in using Duroid 5890 include a small loss tangent, 0.0009 at 10 GHz and ease in machining [9].

3. DESIGN CONSIDERATIONS

In this section, a description of the design procedure for microstrip lines is given. The microstrip-line dimensions were determined using closed-form expressions derived by Hammerstad [10]:

For $W/h \leq 2$,

$$W/h = \frac{8 \cdot \exp(A)}{\exp(2A)-2} \tag{5}$$

For $W/h \geq 2$,

$$W/h = \frac{2}{\pi}\left[B-1-\ln(2B-1) + \frac{\epsilon_r-1}{2\epsilon_r}\left\{\ln(B-1)+0.39 - \frac{0.61}{\epsilon_r}\right\}\right] \tag{6}$$

where

$$A = \frac{Z_o}{60}\sqrt{\frac{\epsilon_r+1}{2}} + \frac{\epsilon_r-1}{\epsilon_r+1}\cdot(0.23 + \frac{0.11}{\epsilon_r})$$

$$B = \frac{377\pi}{2Z_o\sqrt{\epsilon_r}}$$

A 50 Ω line on 0.031" thick Duroid and with a relative dielectric constant of 2.2 resulted in a strip width of 0.093". Table 2 shows the dimensions of microstrip lines with characteristic impedances of 100, 75, 50, 40 and 30 Ω based upon equations (5) and (6).

Table 2

Microstrip design parameters with h = 0.031"

Z_o	W/h	W (inches)	ϵ_{eff}
30	6.23	.193	1.951
40	4.25	.132	1.907
50	3.08	.093	1.870
75	1.59	.049	1.805
100	0.89	.028	1.758

To complete the design, the length of the microstrips had to be determined. The dimensions of the circuit boards had to be small to minimize loss through the guide, while, at the same time, it had to be long enough to ensure that any perturbations in the guide fields were confined to the vicinity of the discontinuity under study. In addition, field perturbations, caused by the connectors and coaxial to microstrip transitions, had to be minimized. The attenuation constant for the lowest non-TEM mode was computed by Farr using a spectral Galerkin technique, and it proved to be greater than 50 dB/cm at 10 GHz [11]. For a 2 cm long section, this attenuation constant provided sufficient resolution between the individual step discontinuities. Figure 2 shows the microstrip lines used in the experiment. Sections with characteristic impedances of 100, 75, 40 and 30 Ω were inserted in series with the 50 Ω line; referring to Figure 2, note that lines C through F have 2 cm long center sections, whereas line B has a 1.25 cm center section. This line was used to show how isolation between discontinuities depended on their separation. The measuring system was based on a 50 Ω reference. Similarly, to isolate the discontinuity effects created by the connectors, line segments leading to the discontinuity were made 2.81 cm long. Thus, the overall length of the microstrips was 7.60 cm. For improved accuracy, the microstrips were etched using photolithography and were gold plated.

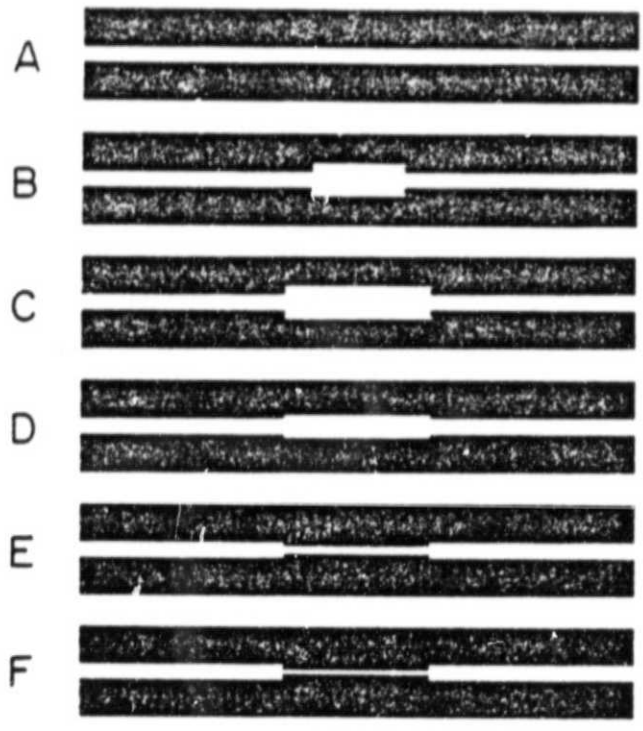

Figure 2. Microstrip patterns printed on Duroid: A) 50 Ω line, B) 30 Ω short section, C) 30 Ω section, D) 40 Ω section, E) 75 Ω section, F) 100 Ω section.

The test fixture, shown in Figure 3, was designed to within the specified tolerance of 0.002". A flanged seal was included for shielding and for simplicity in aligning the boards during assembly. The microstrip boards were firmly pressed against the ground plane to insure good electrical connection and uniform thickness. The connectors utilized belong to the Wiltron K-Connector series. The sparkplug female K102-F:SP42 connector proved to be ideal for this application due to its outstanding electrical and mechanical performances [12],[13]. As suggested by Oldfield [14], the center pins were custom made to provide for an optimum transition from the coaxial line to the microstrip. The custom-made center pins, supplied by Wiltron, had a diameter of 0.040" and were gold plated. It has been found that the diameter of the pin had to be equal, or no less than one-third the microstrip line width [15]. A good transition was obtained by soldering the 0.040" diameter pin onto the 0.093" wide microstrip line. In addition, a short section of the air line and a gap between the microstrip board and the wall of the fixture provided the required matching for the transition from coaxial cable to the microstrip. The air line was designed using the known result for coaxial cables [16]; the outer diameter of the 50 Ω line is 2.3 times the inner one. For a 0.040" pin, the outer diameter is 0.092". These simple modifications were recommended by Wiltron in their assembly instructions [17]. To insure repeatability, the connectors were adjusted using a torque wrench.

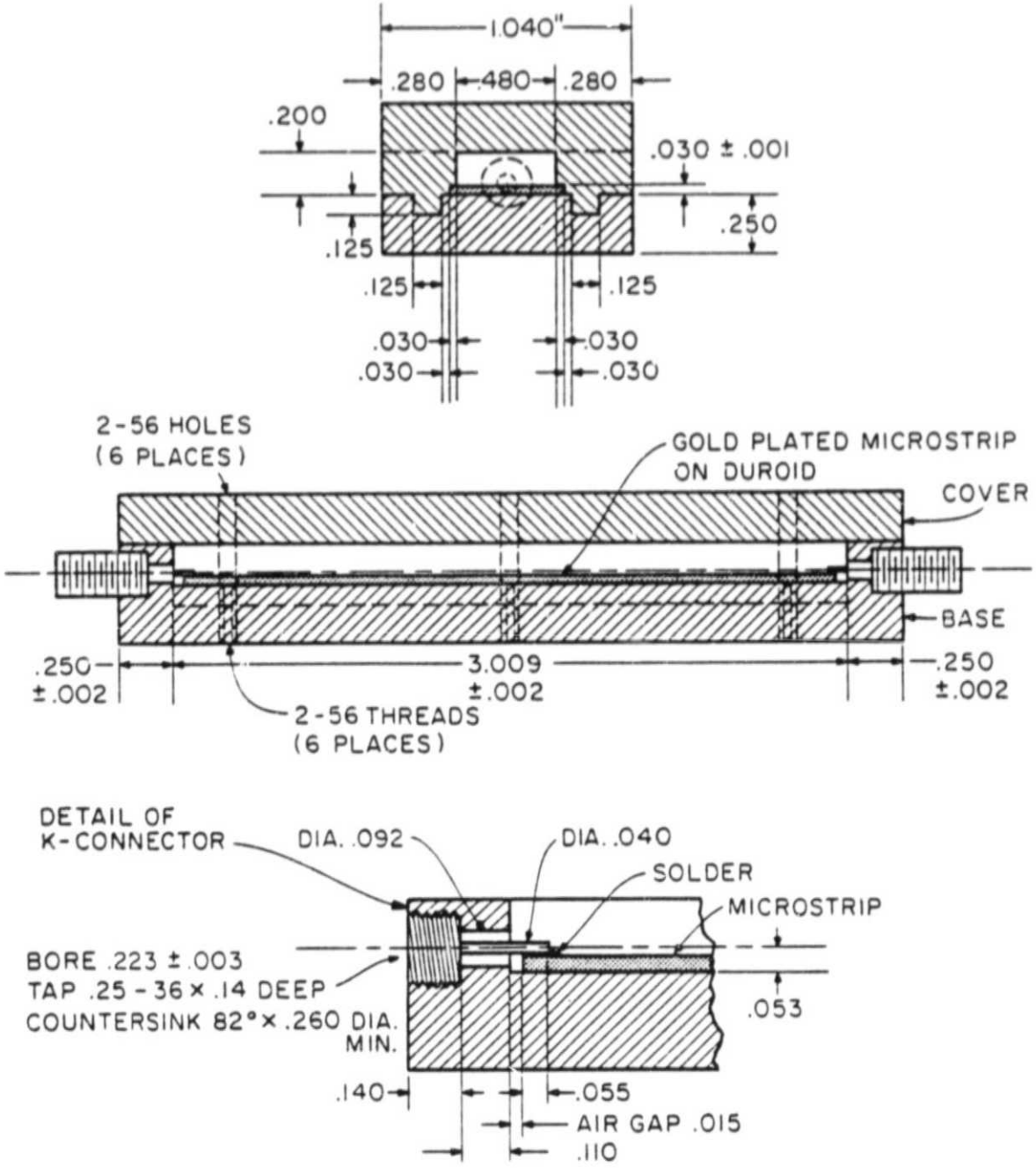

Figure 3. Machine drawing of test fixture. Note 0.015" compensation gap; this provides matching between connector and microstrip. All dimensions are in inches.

Delicate handling, mounting, and soldering of components were employed during the assembly stages. In order to fully utilize the potential of the test fixture, the parts were thoroughly cleaned in ethanol and aligned with a 0.015" thickness gauge. The pins were then carefully soldered using a fine tip iron and high temperature solder. To increase the flexibility of the setup, the fixture was provided with interchangeable microstrip boards and connectors. The assembly process was completed as shown in Figure 4.

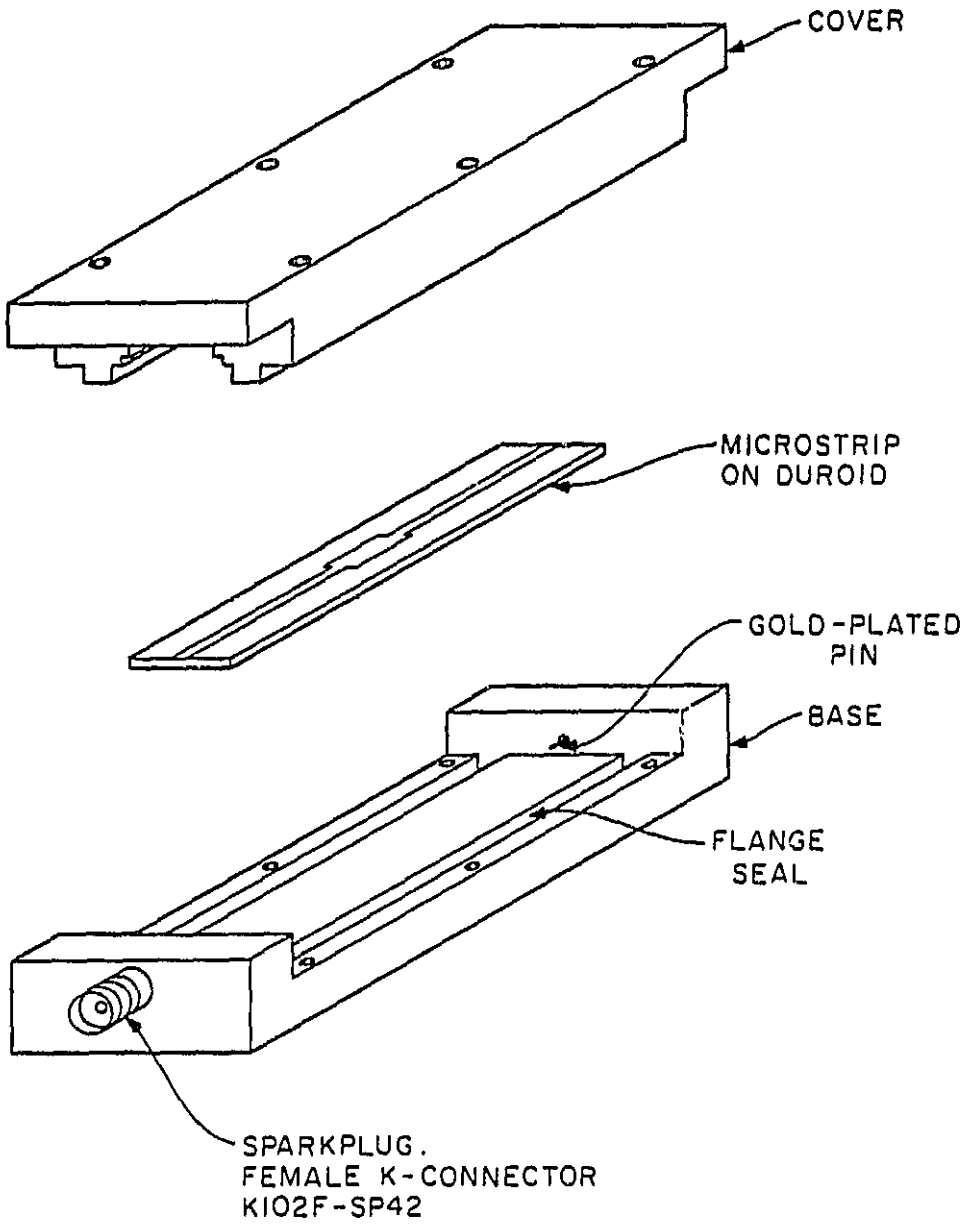

Figure 4. Assembly drawing of test fixture. Note flanged seal to avoid radiation to the outside. Also note that cover presses board tightly onto base.

4. MEASUREMENT PROCEDURE

The test setup utilized throughout this project included sophisticated computer-controlled instrumentation. Preliminary designs and evaluation of performance tests were made on an HP8408 Automated Network Analyzer (ANA) system. During the final stage of the study, more accurate and thorough measurements were made on an HP8510 ANA system. These systems provided reliable operation up to 18 GHz. A block diagram of the test setup utilized is shown in Figure 5.

A series of full band measurements for the various microstrip lines was carried out. The system was calibrated at 401 data points ranging from 45 MHz up to 18.045 GHz. The 18 GHz range contains all integer multiples of the 45 MHz fundamental frequency as required for computing the inverse Fast Fourier Transforms in the time-domain analysis. A precision APC-7mm calibration kit, consisting of open- and short- circuit terminations and fixed and sliding loads, was used to start up the system. All adjustments were made using calibrated torque wrenches.

One of the most significant aspects of this experimental study has been the evaluation of the microstrip discontinuities in the time domain. This measurement simulated the traditional time-domain reflectometer measurement and presented information useful in determining the types of discontinuities present, whether they were resistive, inductive or capacitive [18]. From the reflection data obtained, the corresponding time domain

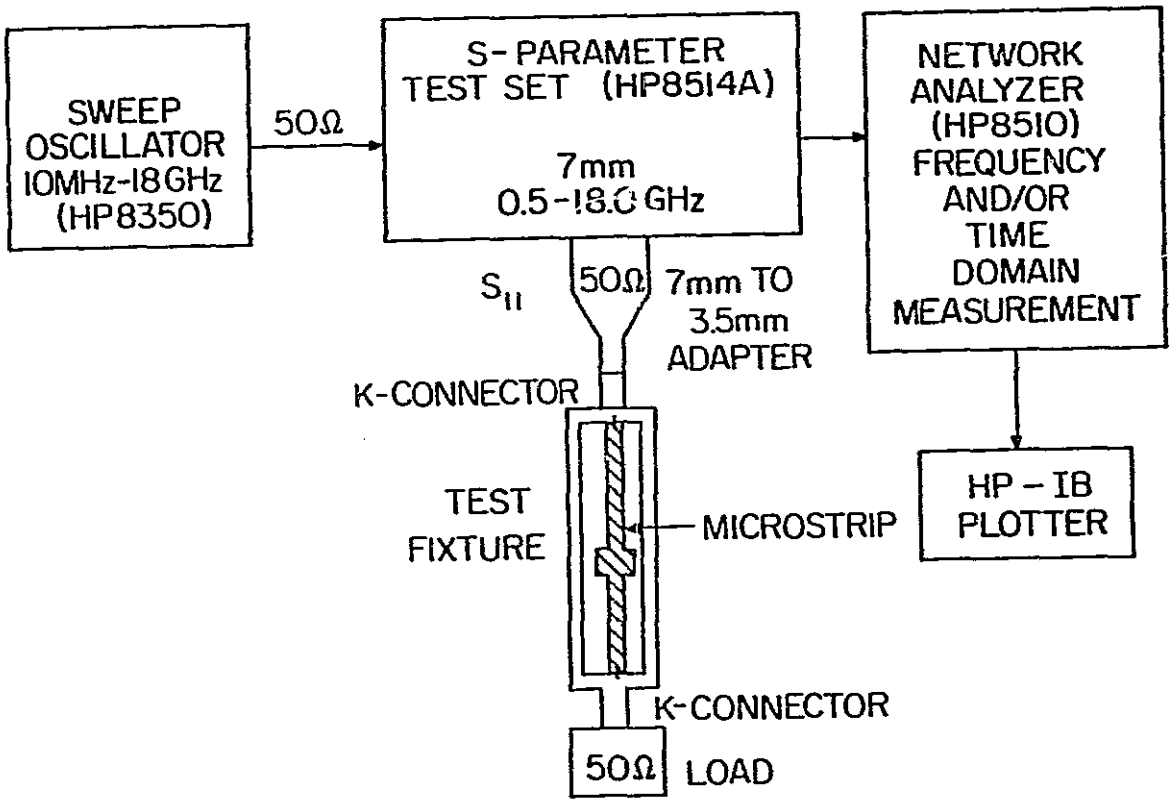

Figure 5. Block diagram of the test equipment used to measure the reflection coefficient and return loss of the microstrip lines.

responses could be interpreted using conventional time-domain reflectometer techniques with precision and high-resolving power [19].

The frequency-domain return loss measurement is a composite response of all the discontinuities present in the line. To obtain the time-domain response, the inverse Fast Fourier Transform of the data was mathematically calculated. The internal high-speed computer in the HP8510 made this calculation using Chirp-Z FFT computation techniques [20]. The resulting measurement was the fully error-corrected, time-domain reflection response of the microstrip displayed in near real time [21]. The time-domain measurement showed the effects of each individual discontinuity as a function of time, i.e., connectors, and step change in impedance. This, in turn, could be interpreted as the position along the line by multiplying the scale by the propagation velocity along the guide.

In order to enhance the time-domain measurements, a gating function, internal to the HP8510, was utilized. This feature gave added flexibility in selectively removing individual responses in the time domain. The effects of the connector-to-microstrip transitions were removed, while preserving the response of the line. The gate utilized, shown in Figure 6, is a time filter with a bandpass filter shape. In converting the data back to the frequency domain, the effects of the responses outside the gate were removed. The data enhancement was achieved, however, at the expense of an increased step rise time. The rise time, in turn, was dependent upon the bandwidth of the measurement and was

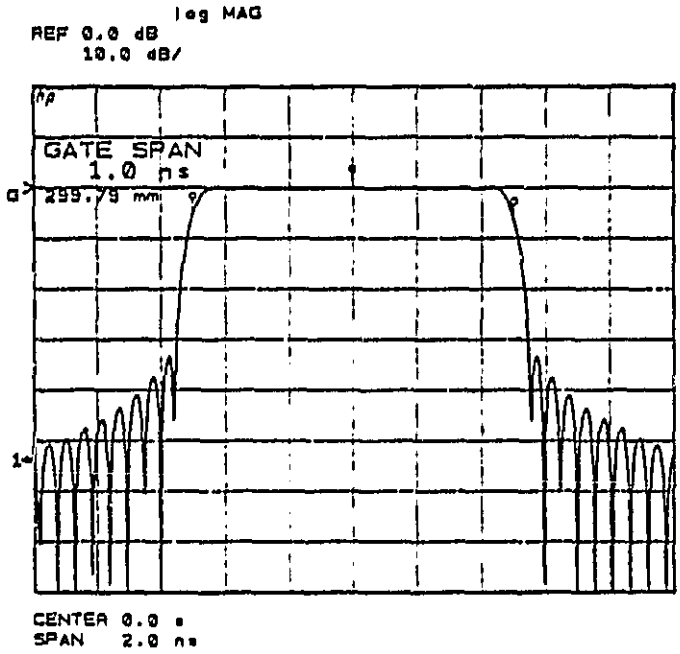

Figure 6. Shape of gate in time domain. Gate start and stop indicate -6 dB cutoff times.

calculated using an approximate formula given by Hewlett-Packard [22].

For a normal window shape and for a frequency range from 45 MHz up to 18 GHz:

$$\text{STEP RISE TIME} = \frac{0.99}{\text{FREQ. SPAN}} \qquad (7)$$

$$= 55 \text{ psec}$$

The corresponding space resolution for this rise time was $v_p \times$ STEP RISE TIME= (55psec) $\times$ (2.19×10^{9}) = 1.2 cm.

Some of the side effects of this technique were increased sidelobes, overshoot, and ringing in the time-domain step stimulus. It is important to point out that the frequency-domain measurement was bandlimited to 18 GHz, and, thus, caused the slight distortion in the time-domain response. Also, the presence of the non-TEM modes above 12 GHz produced added distortion of the time and frequency responses; thus, special care was taken in evaluating these responses. The passband ripple and sidelobe levels are descriptive of the gate shape; for the normal shape gate the specified values were ±0.04 dB of passband ripple and a sidelobe level of -45 dB. For best results and minimum distortion with the gating, it was necessary to center the gate around the desired response and to make the gate span wide enough to include all of those responses.

5. DATA ANALYSIS

The microstrip lines designed were evaluated using the experimental methods outlined in Chapter 4. The 50 Ω line was examined first, and some of the assumptions made during the design process were validated.

The total loss through the line was evaluated using a substitution measurement [23]; Figure 7 shows a plot of the return loss for the 50 Ω microstrip terminated in a short circuit. Alternatively, the plot could be interpreted as the loss incurred in a round-trip through the line; the loss incurred in traversing the line once could then be read off the plot and divided by two. Up to 12 GHz, the losses remained under 0.4 dB. The value calculated in section 2.4 was 0.23 dB; it included the effects of dielectric and conductor losses but excluded the effects of mismatch losses.

Throughout the rest of the report, the reflection measurement data are presented in both the time and frequency domains. These responses can be related through the Fourier Transform.

The magnitude of the return loss for a full band measurement from 45 MHz to 18.045 GHz for the 50 Ω line is displayed in Figure 8a. The pattern shown in this plot corresponds to the characteristic beating of two identical discontinuities connected to the ends of a transmission line, i.e., the connector-to-microstrip transitions.

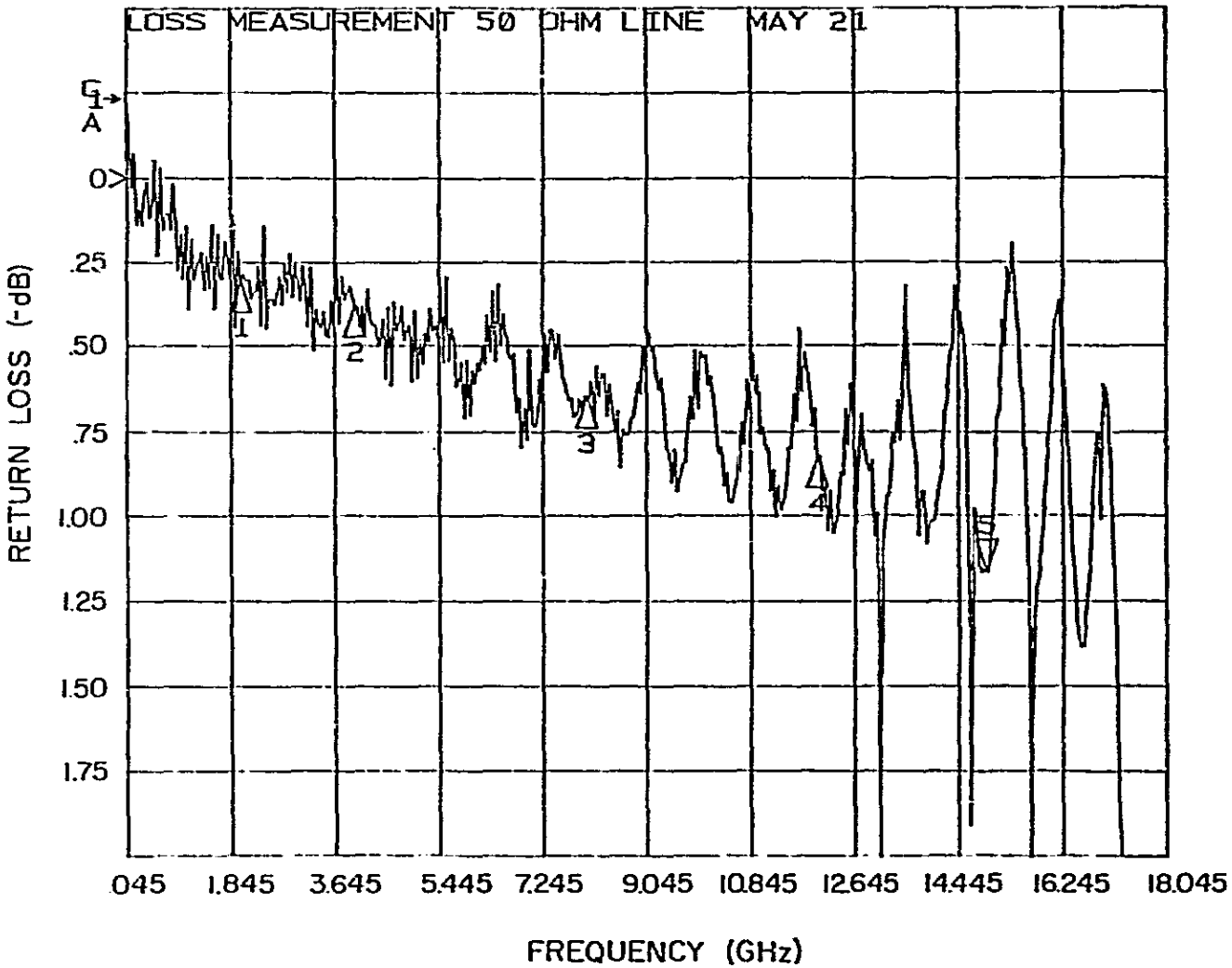

Figure 7. Return loss for 50 Ω microstrip with a shorted termination. Up to 12 GHz, loss remains under 0.4 dB (divide by two the value read off the plot). Note the sharp peaks due to non-TEM modes propagating above 12 GHz.

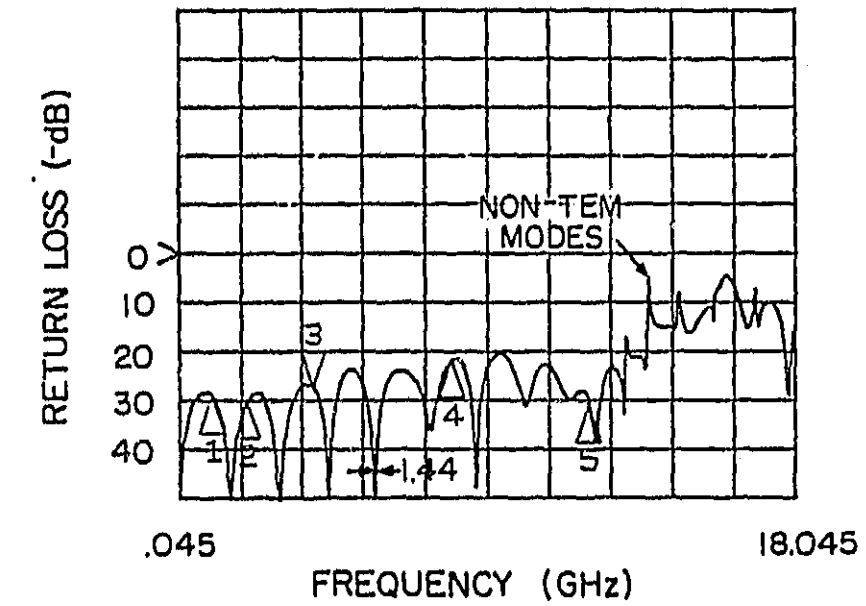

(a)

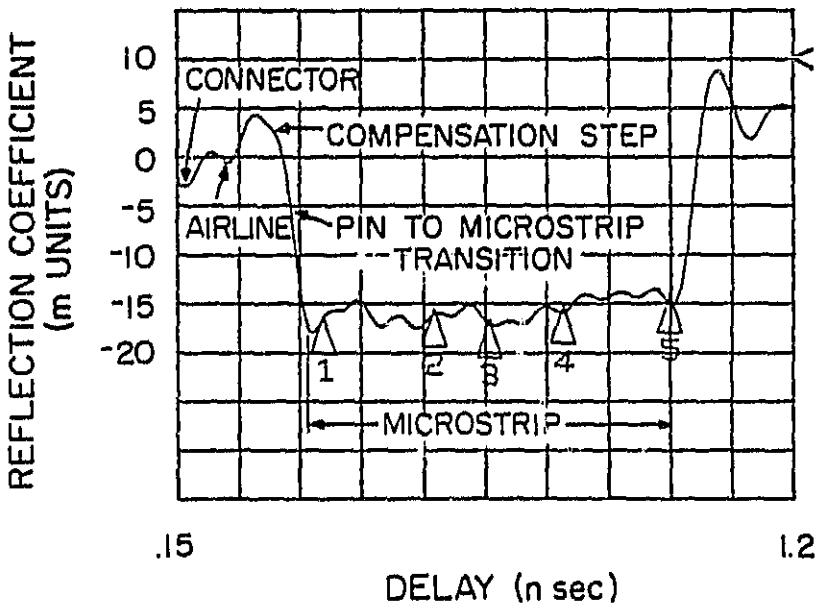

(b)

Figure 8. Reflection response of 50 Ω line: a) Return loss in frequency domain, b) Reflection coefficient in time domain.

The separation between the nulls was computed using a result for transmission lines [24]. For a line of lenght L and with a propagation velocity of V_p, the nulls in the return loss occur at frequencies where the electrical length of the line is a multiple of a quarter-wavelength, namely,

$$f = N \frac{V_p}{2L} \tag{8}$$

For a 7.62 cm line, and a $V_p = 2.2 \times 10^8$ m/s, the nulls occurred at 1.44 GHz intervals. This value coincides with the observed pattern.

The return loss pattern displayed in Figure 8a was better than -20 dB up to 12 GHz. For frequencies above that, non-TEM modes start to propagate, and appear as sharp peaks at the upper end of the return loss range. These modes were excited at frequencies for which the guide dimensions became comparable to the guide wavelengths.

The details in the trace for the corresponding time-domain response, shown in Figure 8b, deserve further explanation. This time-domain response could be more easily interpreted by proceeding from left to right, i.e., corresponding to position along the line. The system's flat 50 Ω reference was present until the K-connector was reached; as specified by Wiltron, very small reflections were observed [25]. The short section of 50 Ω airline that followed produced some added ripple. This ripple increased once the compensation gap was reached, and which, in turn, made the free-floating connector center pin look inductive;

this is shown by the rise in the trace. Once the microstrip was reached, a 20 mUnit drop in the trace occurred, and was due to the capacitive nature of this type of transition. This capacitance was largely determined by two factors: a step in the groundplane from the circular coaxial geometry to the rectangular microstrip geometry, and the step associated with the change in cross-section of the center conductor [26]. After traversing the microstrip, similar effects occurred at the other end, but in the reverse order.

During the design procedure, it was observed that the closed-form expressions (5) and (6), used in calculating the microstrip widths, resulted in slightly lower characteristic impedance than desired. For this reason, the reflection coefficient for the 50 Ω microstrip was 0.02, instead of 0; this value is still equivalent to a -35 dB return loss, which, by all practical standards, is very good for a planar waveguide.

In an attempt to isolate the response of the microstrip line, shown in Figure 9a, the gating feature on the system was utilized. The electrical length of the guide was calculated so that the gate could be placed directly at the ends of the microstrip, between the two connectors; their location is shown in Figure 9b. It should be noted that the response outside the gate stays constant at the level corresponding to a 50 Ω line.

Referring back to the filtered return loss for the 50 Ω microstrip line, shown in Figure 9a; the beating pattern was preserved, but with an improvement of 8 dB in the return loss.

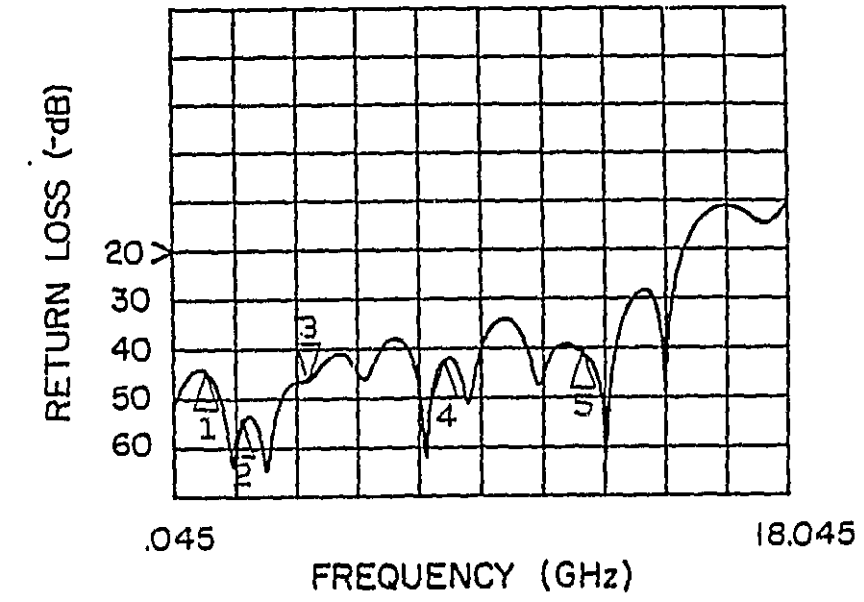

(a)

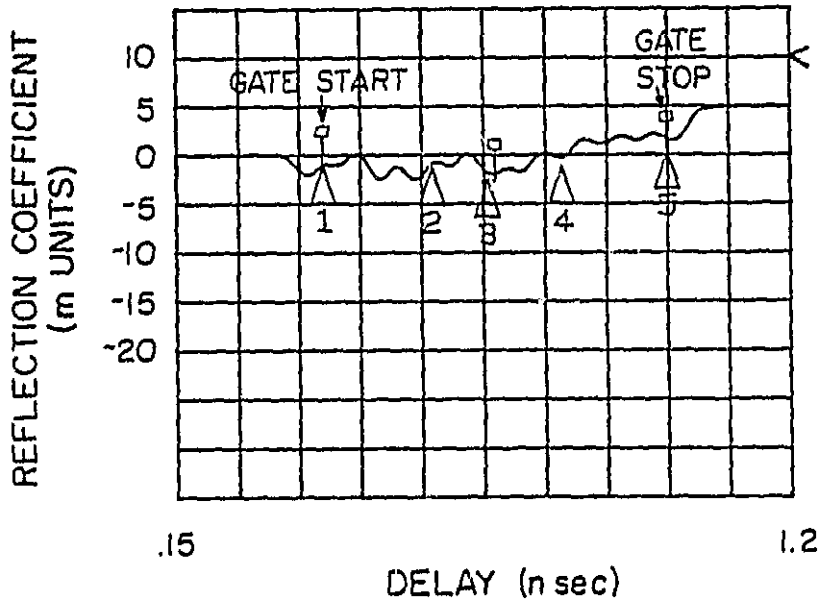

(b)

Figure 9. Gated reflection response of 50 Ω line: a) Return loss, b) Reflection coefficient.

The transitions studied were classified by the relative magnitude of the impedance step. The step-down cases, as with the 30 and 40 Ω sections, were capacitive in nature and were modelled by a shunt capacitance, with an equivalent circuit shown in Figure 10a. This equivalent circuit includes all discontinuities in the line. Conversely, the step-up cases, as with the 75 and 100 Ω sections, were inductive in nature; this abrupt decrease in width was modelled by a series inductance [27]. The T-section equivalent circuit is shown in Figure 10b.

To complete the study, the different impedance steps in the microstrip lines were analyzed. The presence of the 30, 40, 75, and 100 Ω section discontinuities in the line produced very noticeable results, which are presented in Figures 11 through 19.

From the observed time-domain responses, the lower-impedance sections, 30 and 40 Ω, produced a downward deflection of the trace, whereas the higher impedance sections, 75 and 100 Ω, produced an upward deflection of the pulse. The sharp edges were effectively smoothed out by the junction capacitance and, thus, no abrupt level changes were observed.

The responses followed the same trends as those for the 50 Ω line but with a few peculiarities. Considering the responses in the frequency domain first, the beating pattern was still present, with the separation of nulls of 5.44 GHz, corresponding to the 2 cm discontinuity sections of the line. The non-TEM mode peaks were still present at frequencies above 12 GHz; these were dependent only upon the cavity dimensions and not upon the type of discontinuity on the line.

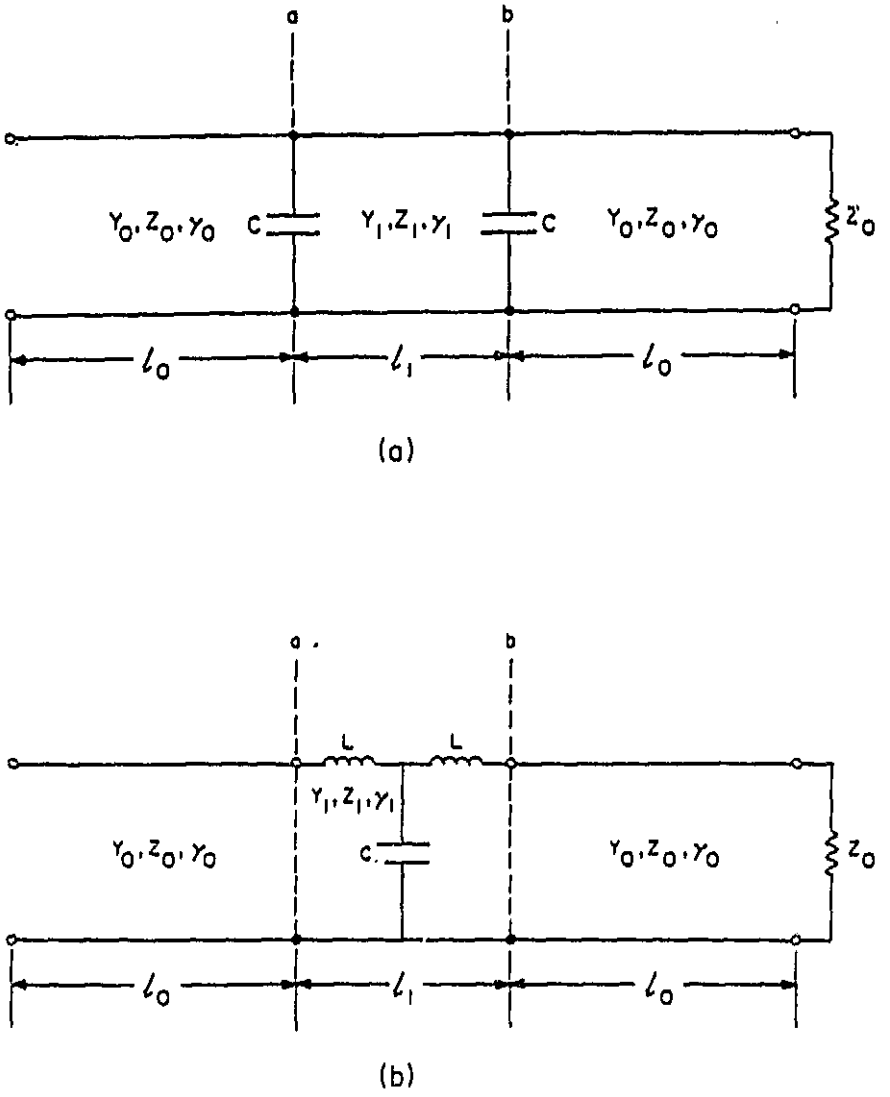

Figure 10. Equivalent circuits for discontinuity in microstrip:
a) Capacitive model, when $Z_1 < Z_0$.
b) Inductive model, when $Z_1 > Z_0$.
L_1 = 2 cm, L_0 = 2.81 cm, Z_0 = 50 Ω.

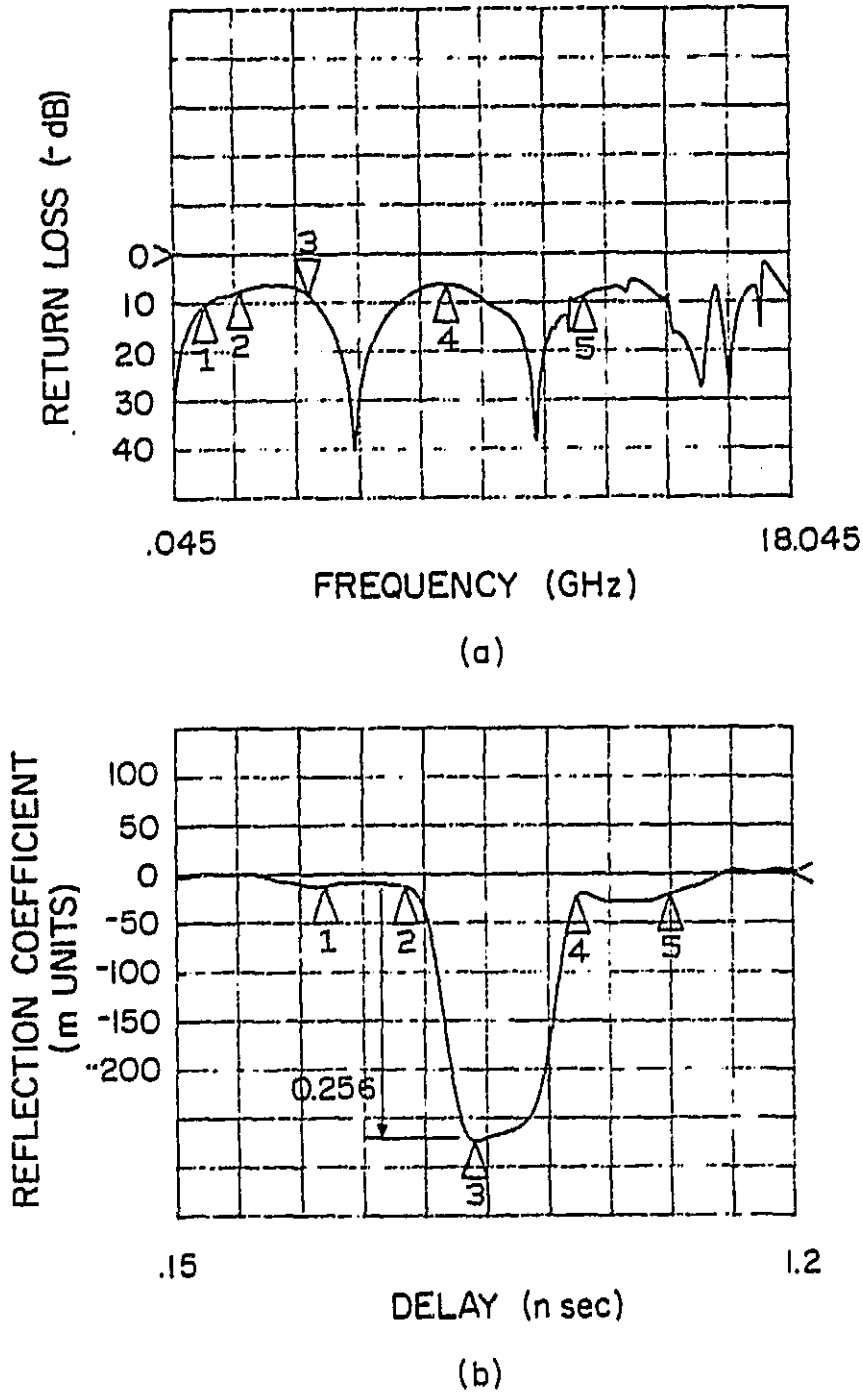

Figure 11. Reflection response of 30 Ω line: a) Return loss, b) Reflection coefficient.

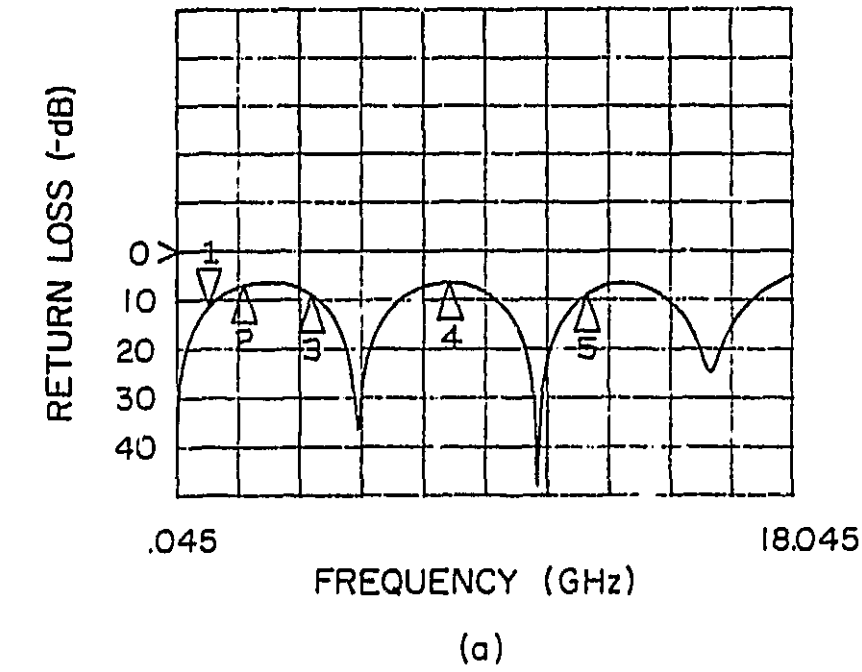

(a)

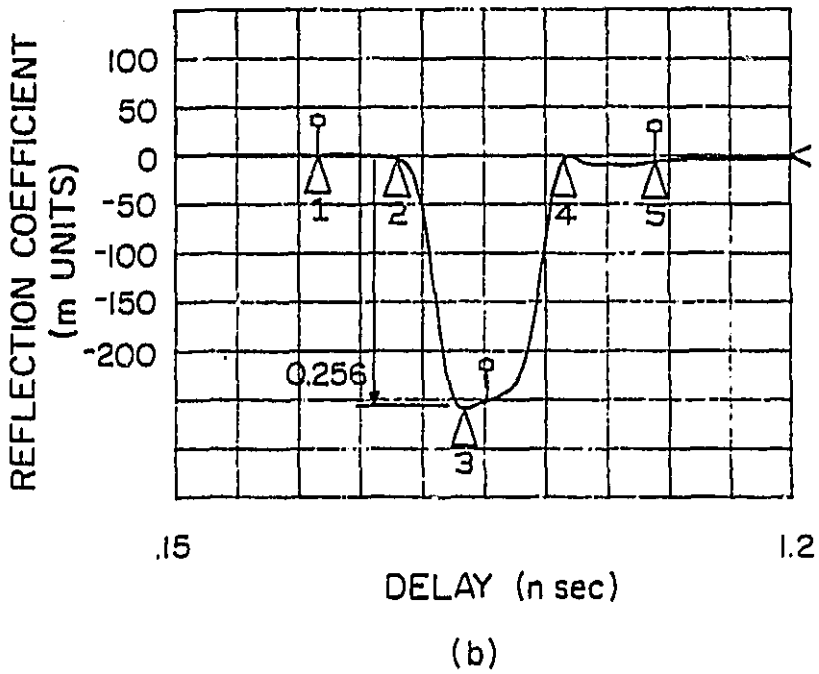

(b)

Figure 12. Gated reflection response of 30 Ω line: a) Return loss, b) Reflection coefficient.

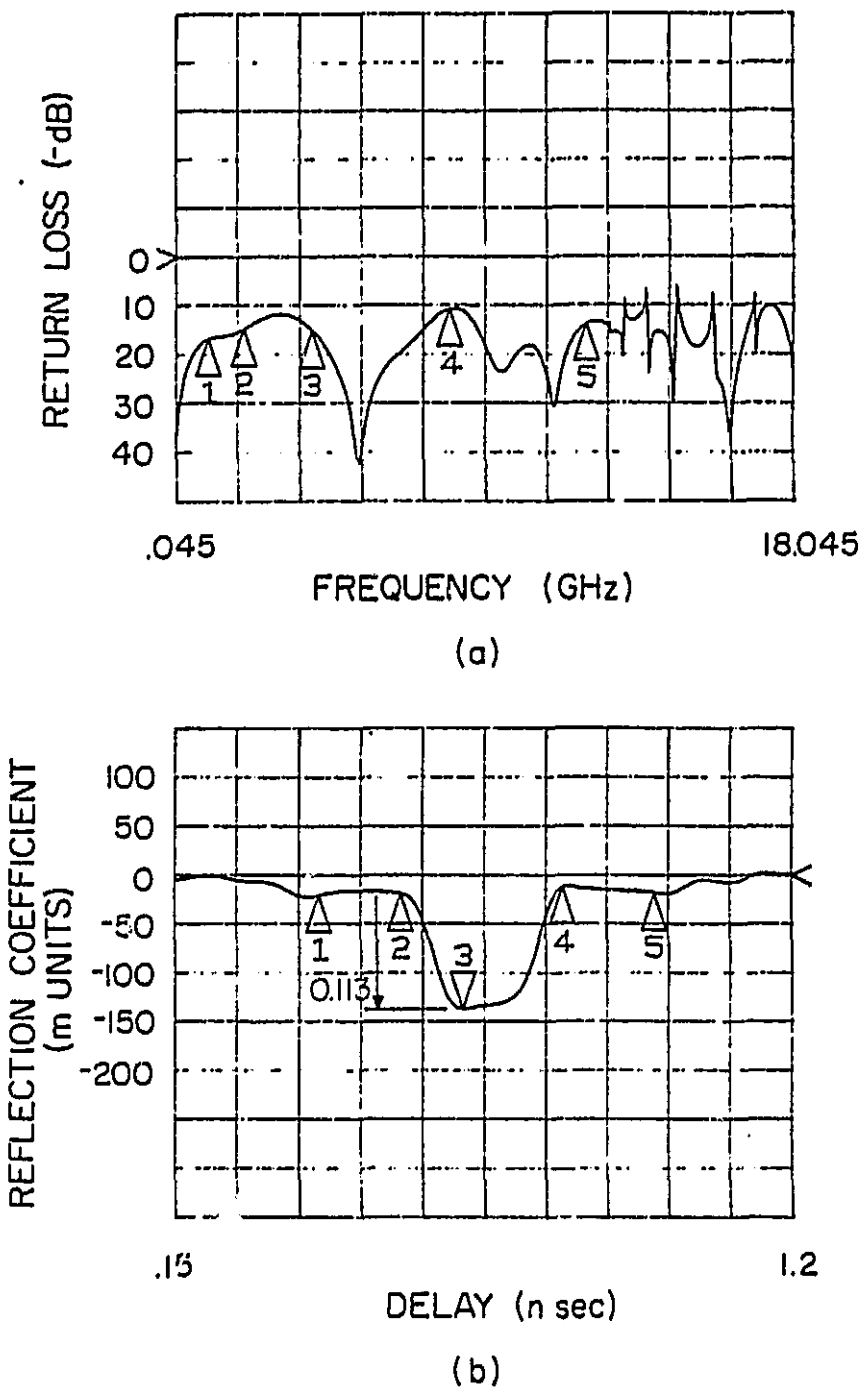

Figure 13. Reflection response of 40 Ω line: a) Return loss, b) Reflection coefficient.

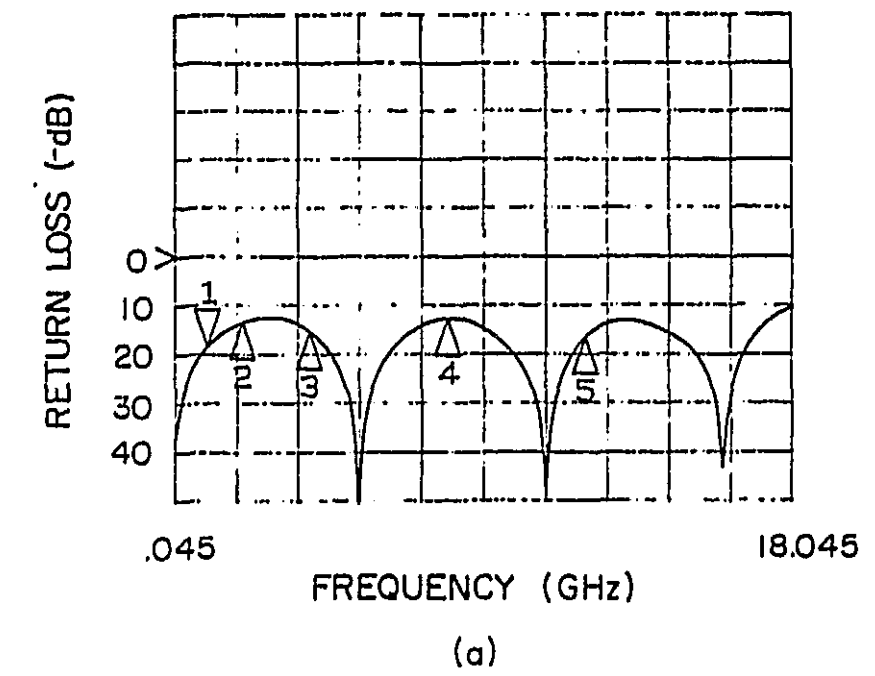

(a)

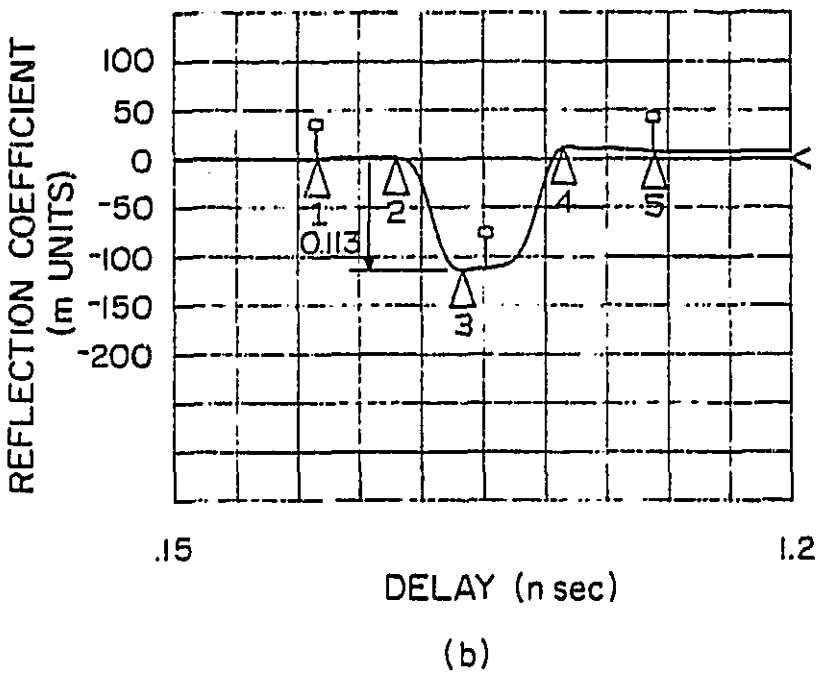

(b)

Figure 14. Gated reflection response of 40 Ω line: a) Return loss, b) Reflection coefficient.

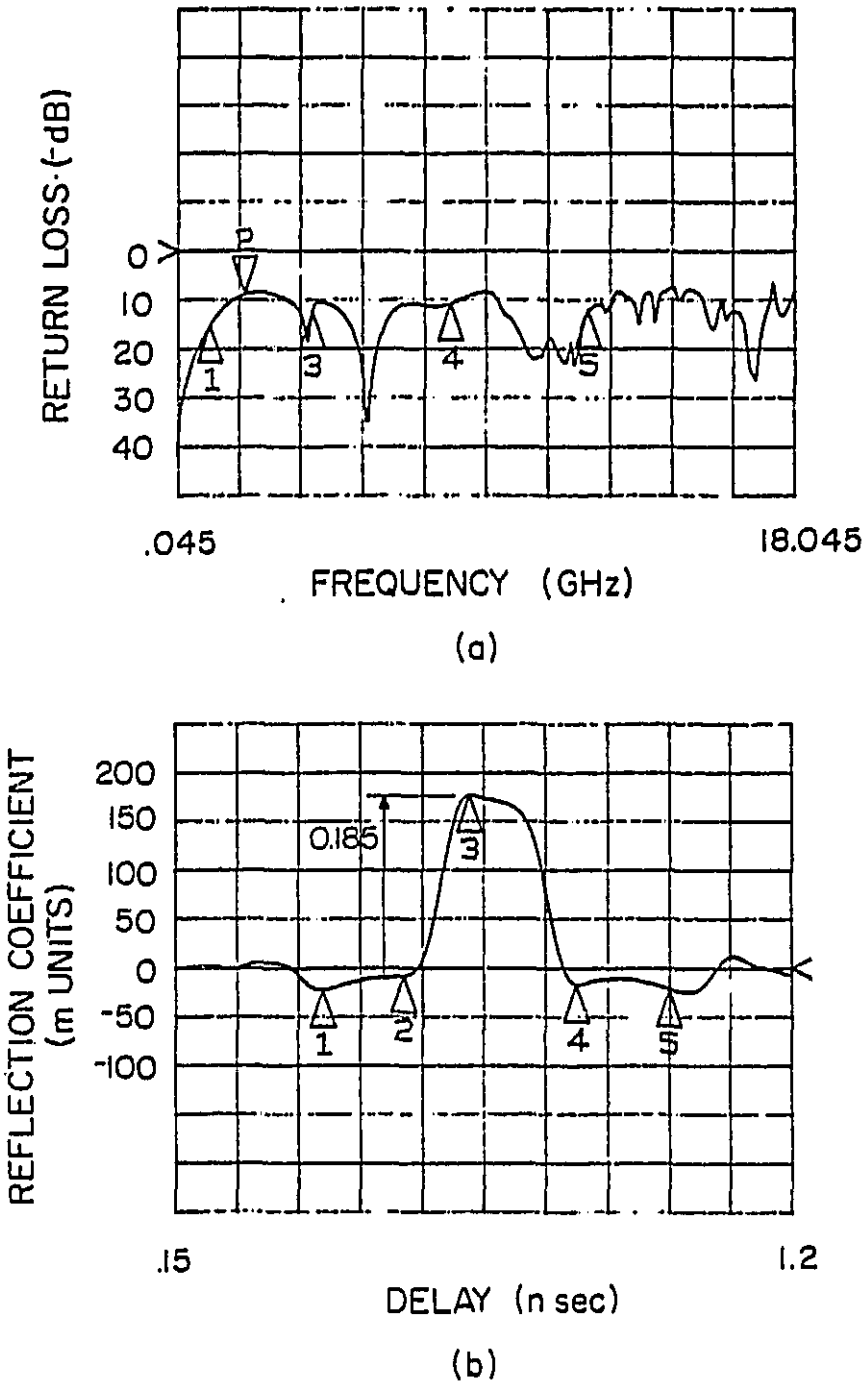

Figure 15. Reflection response of 75 Ω line: a) Return loss, b) Reflection coefficient.

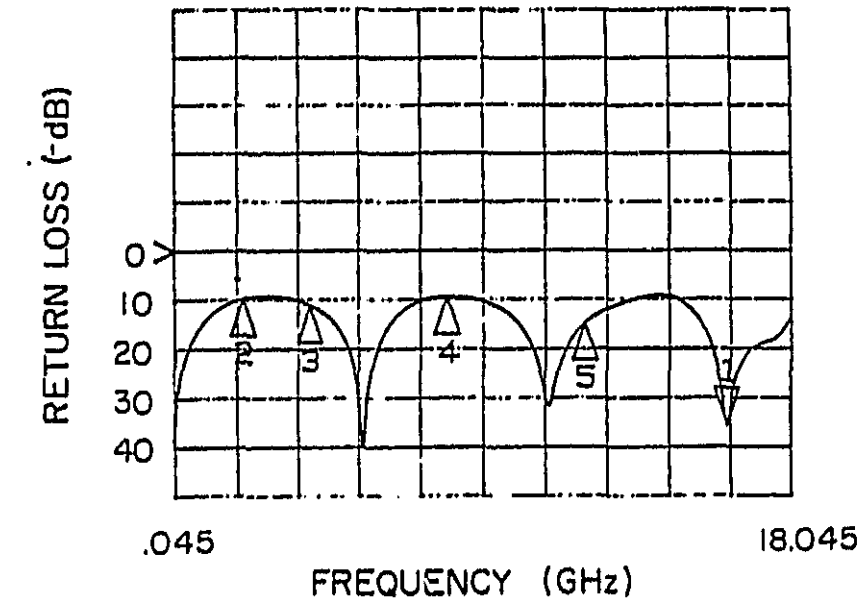

(a)

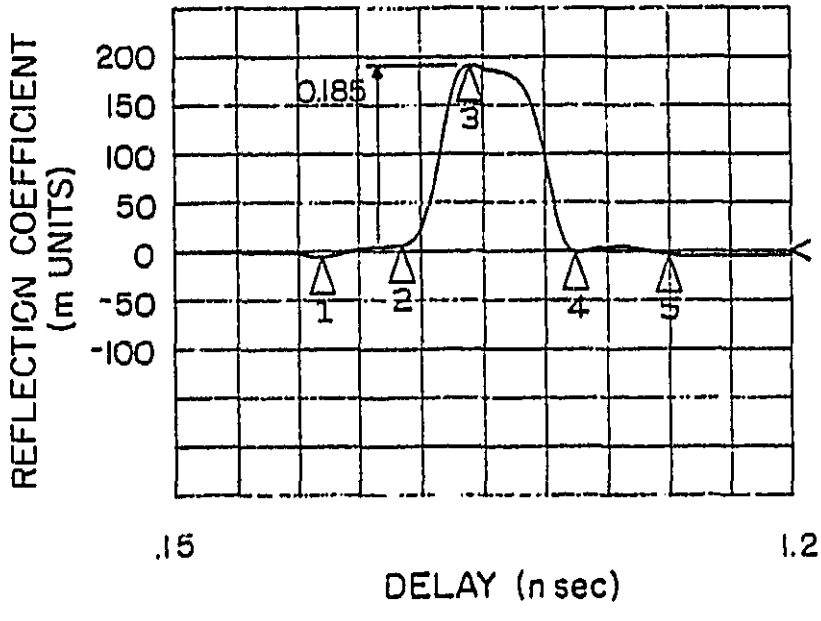

(b)

Figure 16. Gated reflection response of 75 Ω line: a) Return loss, b) Reflection coefficient.

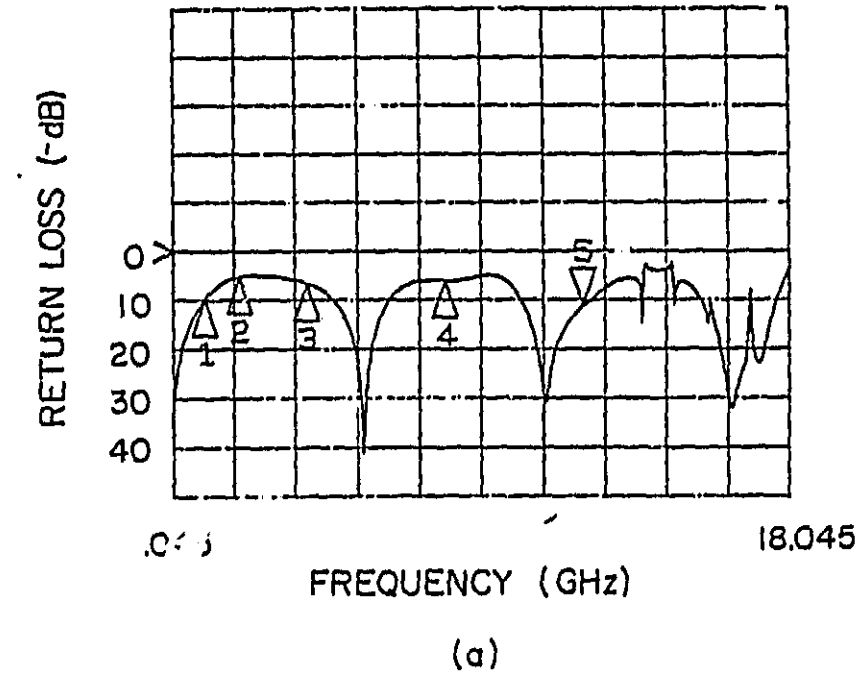

(a)

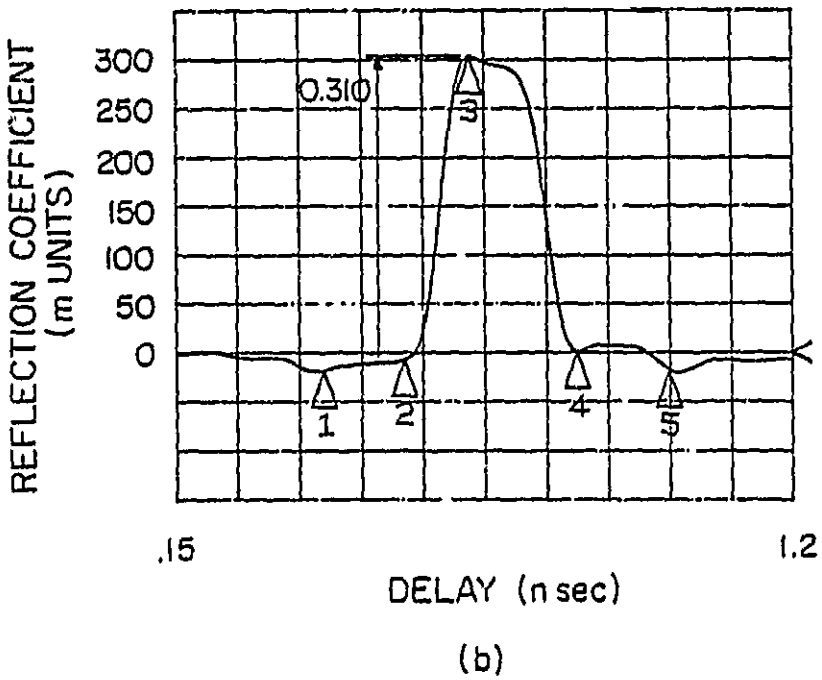

(b)

Figure 17. Reflection response of 100 Ω line: a) Return loss, b) Reflection coefficient.

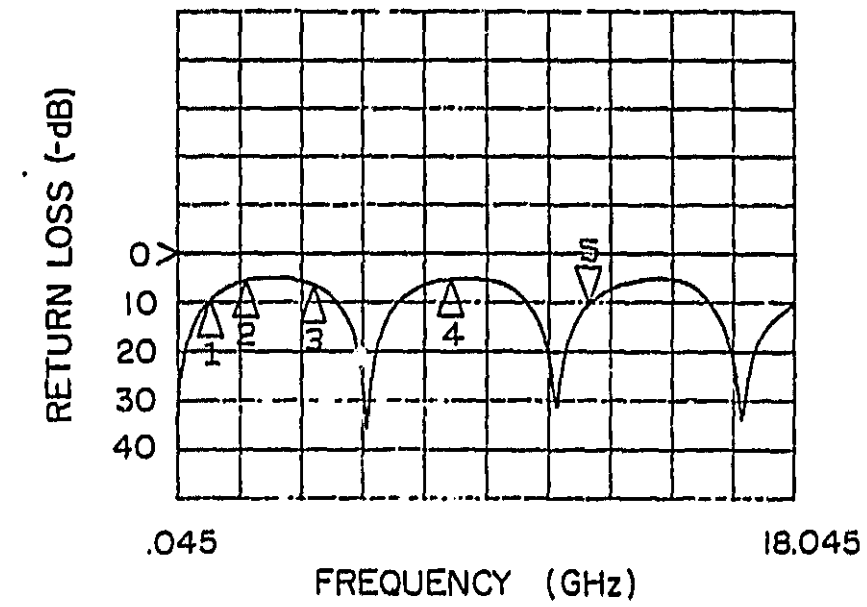

(a)

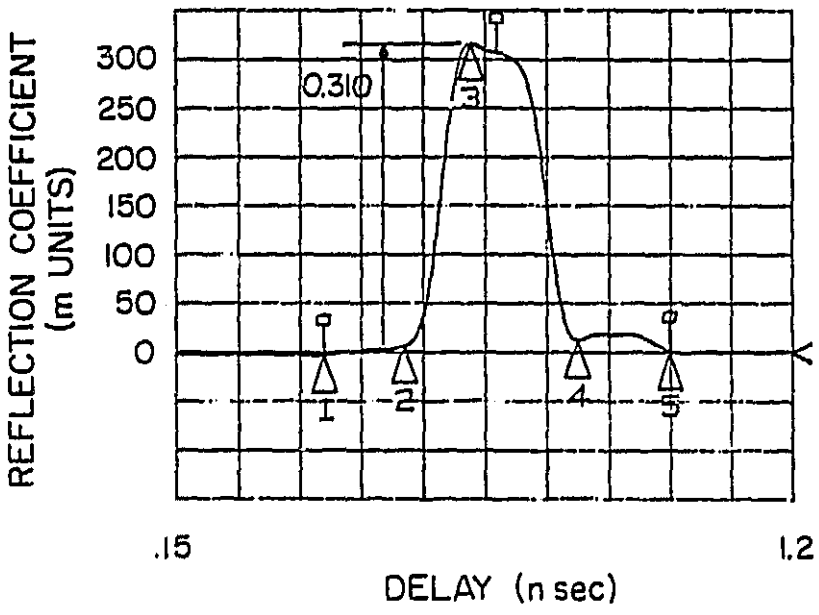

(b)

Figure 18. Gated reflection response of 100 Ω line: a) Return loss, b) Reflection coefficient.

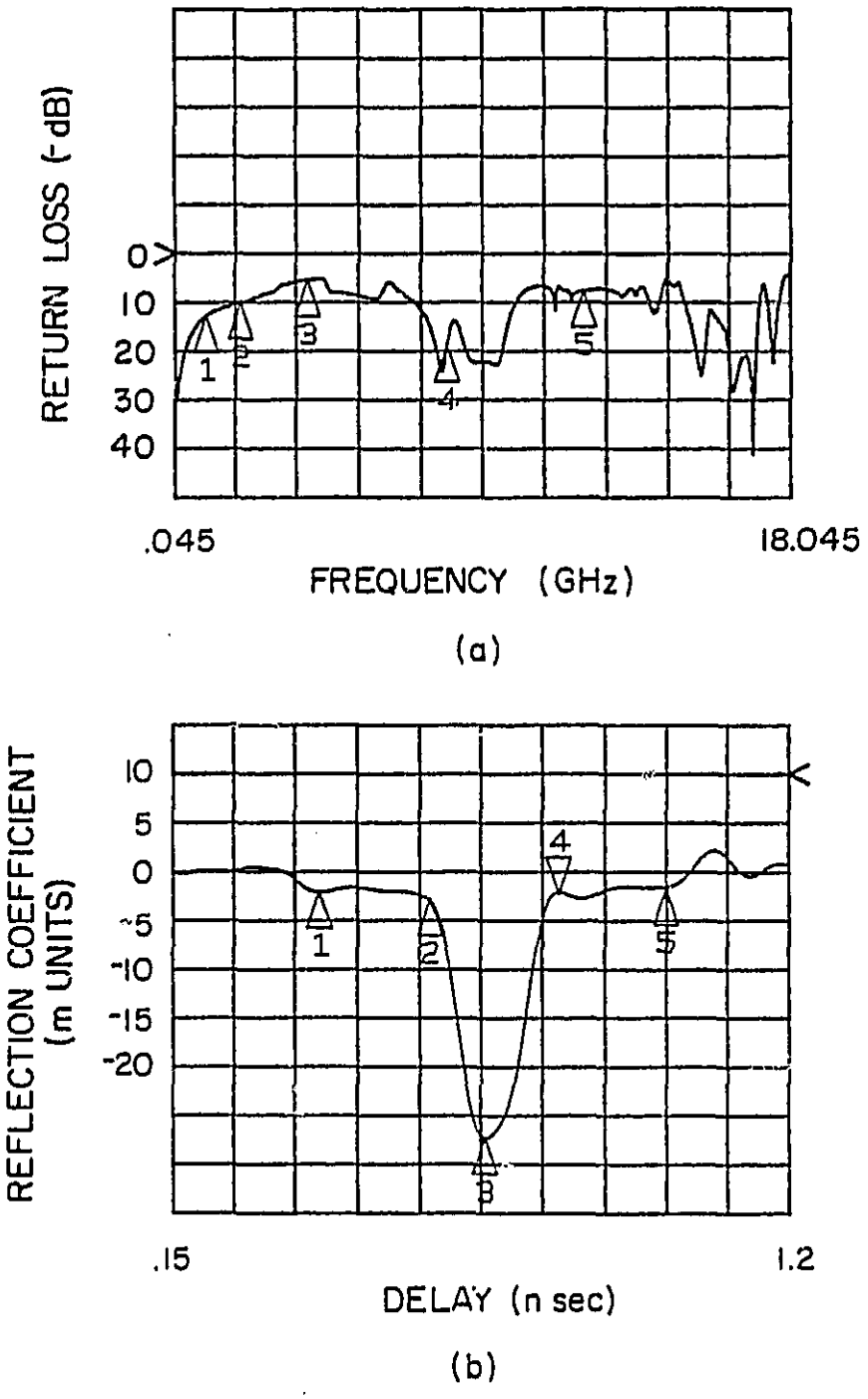

Figure 19. Response fo short section of 30 Ω line. The bottom of the response does not flatten out, as for the case shown in Figure 11.

Consider the time domain data next; the peak magnitudes of the responses corresponded exactly to the values predicted by the transmission line theory shown in Table 3.

Table 3

Calculated and measured reflection coefficients,

Z_o (Ω)	TEM-model	Measured on TDR
30	-0.25	-0.256
40	-0.11	-0.113
50	0.00	-0.020
75	0.20	0.185
100	0.33	0.310

From these measurements, it can be concluded that the magnitude of the discontinuity produced by the impedance steps was significantly larger than that for the other discontinuities in the line, including connectors. Thus, the effects of this discontinuity were predominant in determining the overall reflection characteristics of the microstrip lines.

Using time-domain gating, the responses of the individual discontinuities in the lines were obtained. As expected, the beating pattern is more clearly seen in the return loss; the separation of nulls remained at 5.44 GHz, but with a more periodic and predictable pattern.

To complete this study, the values obtained from the measurements were compared to the values computed by Farr using a mode-matching technique [28] and to the values obtained using a transmission-line model. These results are summarized in Table 4.

Table 4

Return losses, theoretical and experimental.

FREQ. GHz	30Ω	40Ω	75Ω	100Ω
.990	-10.8 ∠-126 -13.2 ∠-125 -11.2	-17.6 ∠-123 -19.2 ∠-123 -18.3	-13.9 ∠ 56 -14.6 ∠ 57 -13.7	-9.1 ∠ 53 -9.6 ∠ 54 -9.4
2.025	-6.8 ∠-160 -8.9 ∠-159 -6.9	-13.1 ∠-157 -14.7 ∠-157 -13.3	-9.5 ∠ 23 -10.1 ∠ 24 -9.5	-5.3 ∠ 21 -5.7 ∠ 22 -5.4
4.005	-8.6 ∠ 140 -10.8 ∠ 139 -8.9	-14.9 ∠ 138 -16.5 ∠ 138 -15.3	-10.7 ∠-37 -11.4 ∠-37 -11.1	-6.1 ∠-32 -6.6 ∠-33 -6.6
8.010	-6.4 ∠-179 -8.3 ∠-179 -6.4	-12.5 ∠-176 -14.0 ∠-176 -12.6	-8.9 ∠ 10 -9.5 ∠ 10 -9.4	-4.9 ∠ 11 -5.3 ∠ 12 -5.2
12.015	-8.9 ∠-141 -10.8 ∠-139 -8.8	-15.9 ∠-133 -17.4 ∠-133 -16.4	-14.3 ∠ 57 -14.8 ∠ 57 -14.7	-10.7 ∠ 59 -11.1 ∠ 60 -10.3

→ Mode Matching
→ Trans. Line
→ Measured

Magnitude dB ∠(degrees)

For all cases, there was excellent agreement between the experimental results and the mode-matching results, better than 5% correspondence. The results obtained from the transmission-line model differed from the others because the model does not account for the junction capacitance. For this reason, it is believed that these experiments were very accurate at the operating range up to 12 GHz.

6. CONCLUSION

This report has discussed the application of modern design, manufacturing and measuring techniques for the characterization of discontinuities on a microstrip. Results have been presented to show how the type of discontinuity inserted on the line affected the overall response. The return loss patterns observed were periodic in nature, with a separation of nulls proportional to the length of the discontinuity section.

The microstrip reflection characteristics were studied extensively. Special attention was paid to dispersion, loss and non-TEM mode propagation, effects, which were predominant, when the guide dimensions became comparable to the guide wavelengths. Their effects are currently being evaluated, in an effort to extend the range of the experiments up to 18 GHz or above. In selecting the optimal guide configuration, several compromises had to be made in order to obtain the desired response, namely, a convenient frequency range of operation and an adequate substrate material.

Once the substrate material was selected, the design considerations were established. For the purposes of this study, the microstrip had to be placed inside a waveguide. The performance in this type of environment was duplicated by utilizing a closed test fixture with a rectangular cross-section to contain the microstrip. To avoid radiating modes, a flanged seal was included in the design; this configuration provided adequate RF shielding to the outside. To preserve a proper ground

plane interface, the cover overlapped the microstrip board at the edges, pressing it down tightly onto the base. Some time was spent in finding a launcher which provided a good match between the coaxial cable and the microstrip line. It was found that the diameter of the connector center pin should be no less than one third the microstrip line width. The K-connectors proved to be ideal for the configuration under study. To insure uniformity in the assembly of the test fixture, special tools were employed, namely, torque wrenches, thickness gauges and high-temperature soldering iron. For improved electrical performance, the microstrip lines were gold plated and cut precisely for mounting onto the test fixture.

All of the design, assembly and measurement techniques discussed in this report were succesfully applied to this experimental study, resulting in a controlled and reproducible response. The results obtained from these measurements proved to be in good agreement with those computed using a mode-matching technique.

As a continuation of this study, some further experiments, based on the methodology presented in this thesis, include cascaded step discontinuities, gaps in lines, tapered lines, and transitions from one substrate to another. The effects of non-TEM modes of propagation on microstrip performance also deserve further investigation.

REFERENCES

[1] J. Smetana, E.G. Farr, and R. Mittra, "Characterization of MMIC devices for active array applications," NASA Technical Memorandum 86907, September, 1984.

[2] P.J. Meier, "Integrated fin-line millimeter components," IEEE Trans. Microwave Theory Tech., vol. MTT-22, pp. 1209-1215, December 1974.

[3] W.J. Chudobiak, et al., "Dispersion in microstrip," IEEE Trans. Microwave Theory Tech., vol. MTT-19, pp. 783-784, September, 1971.

[4] E.G. Farr, Ph.D. Dissertation, to be published.

[5] G.D. Vendelin, "Limitations on stripline," Microwave Journal, Vol. 13, No. 5, pp. 63-69, May 1970.

[6] E.G. Farr, op. cit.

[7] R.A. Pucel, et al. "Losses in microstrip," IEEE Trans. Microwave Theory Tech., vol. MTT-16, pp. 342-350, Jun. 1968. "Corrections to Losses in microstrip", Ibid.. Vol. MTT-16 pp. 1064, Dec. 1968.

[8] J.D. Welch, and H.J.,Pratt, "Losses in microstrip transmission systems for integrated microwave circuits," NEREM Rec., Vol. 8, pp. 100-101, 1966.

[9] Rogers Corporation, RT/Duroid data sheet, 1981.

[10] E.O. Hammerstad, "Equations for microstrip design," Proc. European Microwave Conference, Hamburg, pp. 268-272, September 1975.

[11] E.G. Farr, op. cit.

[12] Wiltron Co., K-Connector catalog, 1984.

[13] W. Oldfield, "ECM/EW designs to 40 GHz in coax," Microwave System News, June 1984.

[14] W. Oldfield, Wiltron Co., personal communication.

[15] E.H. England, "A Coaxial to microstrip transition," IEEE Trans. Microwave Theory Tech., Vol. MTT-24, No. 1, pp. 47-48, jan. 1976.

[16] S.A. Ramo, J.R. Whinnery, and T. Van Duzer, Fields and Waves in Communication Elctronics. New York: J. Wiley and Sons, 1984, pp. 214-215.

[17] Wiltron Co., op. cit. p. 2.

[18] S.F. Adam, Microwave Theory and Applications. New Jersey: Prentice-Hall, 1969, pp. 457-473.

[19] M.E. Hines, and H.E. Stinehelfer, " Time Domain oscillographic microwave network analysis using frequency domain data," IEEE Trans. Microwave Theory Tech., vol MTT-22, pp. 276-282, Mar. 1974.

[20] A.V. Openheim, and R.W. Schaeffer, Digital Signal Processing. New Jersey: Prentice-Hall, 1975, pp. 321-326.

[21] Hewlett-Packard, "Basic network measurements using the HP8510 ANA system," 1984.

[22] Hewlett-Packard, op. cit. p. 141.

[23] S.F. Adam, op. cit. pp. 379-381.

[24] S.A. Ramo, op. cit. pp.224-226.

[25] Wiltron Co., op. cit. pp.7.

[26] S.J. Nightingale, and M.A.G. Upton, "Three dimensional modelling of some common transitions and interconnections," General Electric technical memorandum, 1984.

[27] P. Benedek, and P. Silvester, " Equivalent capacitances for microstrip gaps and steps," IEEE Trans. Microwave Theory Tech., vol. MTT-20, pp. 729-733, Nov. 1972.

[28] E.G. Farr, op. cit.